PHILOSOPHICAL TRANSACTIONS A

rsta.royalsocietypublishing.org

Research

Cite this article: Dutta-Gupta S, Dabidian N, Kholmanov I, Belkin MA, Shvets G. 2017 Electrical tuning of the polarization state of light using graphene-integrated anisotropic metasurfaces. *Phil. Trans. R. Soc. A* **375**: 20160061.
http://dx.doi.org/10.1098/rsta.2016.0061

Accepted: 22 November 2016

One contribution of 15 to a theme issue 'New horizons for nanophotonics'.

Subject Areas:
optics

Keywords:
active metasurface, graphene, polarization

Author for correspondence:
Gennady Shvets
e-mail: gs656@cornell.edu

Electrical tuning of the polarization state of light using graphene-integrated anisotropic metasurfaces

Shourya Dutta-Gupta[1,5], Nima Dabidian[1], Iskandar Kholmanov[2,4], Mikhail A. Belkin[3] and Gennady Shvets[1,5]

[1]Department of Physics, and Center for Nano and Molecular Science and Technology, and [2]Department of Mechanical Engineering, and Materials Science Program, University of Texas at Austin, Austin, TX 78712, USA
[3]Department of Electrical and Computer Engineering, Microelectronics Research Center, University of Texas at Austin, 10100 Burnet Road, Austin, TX 78758, USA
[4]CNR-INO, Sensor Lab, University of Brescia, via Branze 45, 25123 Brescia, Italy
[5]School of Applied and Engineering Physics, Cornell University, Ithaca, NY 14853, USA

Plasmonic metasurfaces have been employed for moulding the flow of transmitted and reflected light, thereby enabling numerous applications that benefit from their ultra-thin sub-wavelength format. Their appeal is further enhanced by the incorporation of active electro-optic elements, paving the way for dynamic control of light's properties. In this paper, we realize a dynamic polarization state generator using a graphene-integrated anisotropic metasurface (GIAM) that converts the linear polarization of the incident light into an elliptical one. This is accomplished by using an anisotropic metasurface with two principal polarization axes, one of which possesses a Fano-type resonance. A gate-controlled single-layer graphene integrated with the metasurface was employed as an electro-optic element controlling the phase and intensity of light polarized along the resonant axis of the GIAM. When the incident light is polarized at an angle to the resonant axis of the metasurface, the ellipticity of the reflected light can be dynamically controlled by the application of a gate voltage.

THE ROYAL SOCIETY PUBLISHING

Thus accomplished dynamic polarization control is experimentally demonstrated and characterized by measuring the Stokes polarization parameters. Large changes of the ellipticity and the tilt angle of the polarization ellipse are observed. Our measurements show that the tilt angle can be changed from positive values through zero to negative values while keeping the ellipticity constant, potentially paving the way to rapid ellipsometry and other characterization techniques requiring fast polarization shifting.

This article is part of the themed issue 'New horizons for nanophotonics'.

1. Introduction

Manipulation and control of light is of extreme importance for fundamental materials studies, as well as for the development of novel photonic devices [1]. Recently, plasmonic and dielectric metasurfaces (two-dimensional arrays of sub-wavelength structures) have been used for controlling light's properties, such as intensity, phase and polarization [2–7]. The choice of the unit cell as well as the lattice arrangement can be used for defining and controlling the functionality of the metasurface. In many cases, this flexibility, in addition to their small footprint and sub-micrometre thickness, makes metasurfaces either competitive with, or even superior to, conventional optical elements. One of the most appealing potential applications of metasurfaces is for polarization control and tuning. Polarization manipulation is instrumental to several crucial optical applications, such as ellipsometry, polarimetry [8], optical sensing [9] and polarization-division multiplexing [10], which have superior performance compared with conventional methods of material characterization [11] and telecommunication [12]. It has been shown that anisotropic metasurfaces can convert light polarization from linear to circular [13–18], rotate the polarization plane of a linearly polarized light [19–21] and induce asymmetric transmission [6,22,23]. However, most of the studies employed 'passive' metasurfaces: once fabricated, their properties cannot be tuned or controlled. To circumvent this problem, there is an increasing interest in 'active' devices whose optical properties can be dynamically tuned [5,24–32].

The most common approaches to active tuning have been based on mechanical [30,33] motions, thermal (e.g. using phase change materials) excitations [34,35] or electrical [36–39] gating. Among these, electrical control enables higher modulation speed and greater flexibility in device fabrication. Rapid electrical tuning requires incorporation of an electro-optic material that has a short-time response to electrical voltage. Depletion-type semiconductors have been used in the past for terahertz [36] and infrared [37] modulation. More recently, the simplicity of graphene's integration with various substrates and metasurfaces [40,41] is making it the material of choice for optical modulation [24,25,27–29]. While such graphene-integrated metasurfaces have been used primarily for modulating the intensity of the reflected light, recent experiments [29] show that the phase can also be modulated.

A number of exciting applications of phase modulation have been envisioned and demonstrated, such as interferometric motion detection [29] with sub-micrometre resolution and no moving parts. It was also suggested [29] that, by employing a graphene-integrated anisotropic metasurface (GIAM), it may be possible to dynamically control the polarization of light. In this work, using the rotating analyser Stokes polarimetry [6,42] technique, we directly measure the modification of light polarization produced by applying a gate voltage to a GIAM. Specifically, we demonstrate that a linearly polarized (LP) incident light is converted into an elliptically polarized (EP) one upon reflection from a GIAM that supports a Fano resonance for the light polarized along one of its two principal axes. The Stokes parameters of the reflected light are experimentally measured at multiple gate voltages.

The concept of active polarization control realized in this work is illustrated by figure 1, where a graphene-integrated metasurface converts the polarization state from LP (incident) to EP (reflected). The metasurface is fabricated on top of a single-layer graphene (SLG); see Material and methods (§4) for fabrication details. A gate voltage V_g is applied between a silicon back-gate and graphene to tune the ellipticity of the reflected wave via electrostatic doping of the SLG.

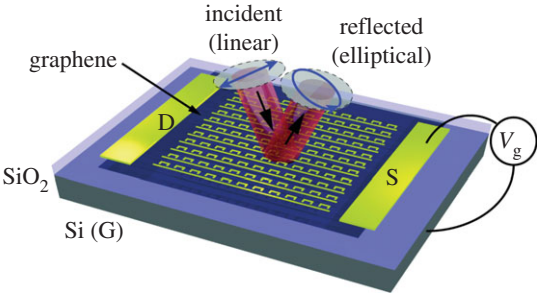

Figure 1. Schematic of the electric control of the polarization state of light using graphene-integrated anisotropic metasurfaces. The incident light is linearly polarized at a finite angle to the principal axes of the metasurface. The reflected light acquires elliptical polarization that depends on the voltage V_g applied between the back-gate (Si) and graphene across an SiO_2 insulating layer. Source and drain electrodes are used to measure graphene's conductivity as a function of V_g.

The metasurface used in this work is essentially the same (i.e. the nominal geometric parameters defined in figure 2*a* are identical) as the one used in [29]. It consists of a two-dimensional array of infinite wires and C-shaped antennas as shown in figure 2*a* for a single unit cell. The anisotropic nature of the metasurface is apparent by observation: the electrically connected wires running parallel to the y-direction provide strong reflectivity of the y-polarized light, but hardly affect the x-polarized one. Moreover, due to mirror reflection symmetry with respect to the (x–z) plane passing through the middle of the C-shaped antenna, it follows from simple symmetry considerations that the polarization-conversion coefficients (from x- to y-polarized and vice versa) vanish: $R_{xy}(\lambda) = R_{yx}(\lambda) = 0$ for all wavelengths. Therefore, the x- and y-axes are the principal polarization axes of the metasurface. Furthermore, because the y-polarized light can excite the electric dipole resonance of the C-shaped antenna while the x-polarized light cannot, the respective $R_{yy}(\lambda)$ and $R_{xx}(\lambda)$ reflection spectra are qualitatively different: the $R_{yy}(\lambda)$ exhibits a strong resonant dip around $\lambda = \lambda_R \approx 7.7\,\mu m$ while the $R_{xx}(\lambda)$ does not possess such a dip.

The origin of the reflectivity dip in $R_{yy}(\lambda)$ is the destructive Fano interference [43] between the broadband response of the wire and the C-shaped dipole [28,29]. Specifically, the current flows in the C-shaped antenna and in the wire are opposite to each other as shown in figure 2*a*, thereby nearly cancelling the overall polarizability of a unit cell of the metasurface. Therefore, only the y-polarization of light excites strong near fields at $\lambda = \lambda_R$. At the resonance frequency, the intensity of the in-plane electric field (which is responsible for the interaction between graphene and the metasurface) in the immediate proximity of the metasurface is enhanced by a large factor $\eta = |E_t^2/E_{inc}^2|$ as shown in figure 2*a*. Both the current distributions and the in-plane field enhancements were calculated at $\lambda = \lambda_R$ for a metasurface without graphene using the COMSOL Multiphysics commercial code.

Because only the y-polarized light, induces strong near-field enhancement of the in-plane electric field component that interacts with graphene's electrons, only the $R_{yy}(\lambda)$ (but not the $R_{xx}(\lambda)$) spectrum is affected by field-effect doping of graphene. The effect of field-effect doping is to inject free carriers (electrons or holes, depending on the gating voltage V_g) into the SLG, thereby affecting its in-plane frequency-dependent conductivity $\sigma_{SLG}(\omega)$, where $\omega \equiv 2\pi c/\lambda$. The standard expression for $\sigma_{SLG}(\omega)$, obtained under the random-phase approximation [44], is provided in the Material and methods section (§4). It relates σ_{SLG} to graphene's Fermi energy E_F, which is itself related to the areal density n of the free carriers in graphene as $E_F = \hbar v_F \sqrt{\pi n}$, where $v_F = 1 \times 10^8\,cm\,s^{-1}$ is the Fermi velocity. As the Fermi energy increases, graphene behaves as an increasingly inductive [24,41] element that causes the blue-shifting of the resonance frequency as shown in figure 2*d*, where the simulated reflectivity R_{yy} for three different (colour-coded) Fermi energies are depicted as solid lines. Graphene does not affect $R_{xx}(\lambda)$, so it is plotted as a single dashed line assuming that graphene is not present underneath the metasurface.

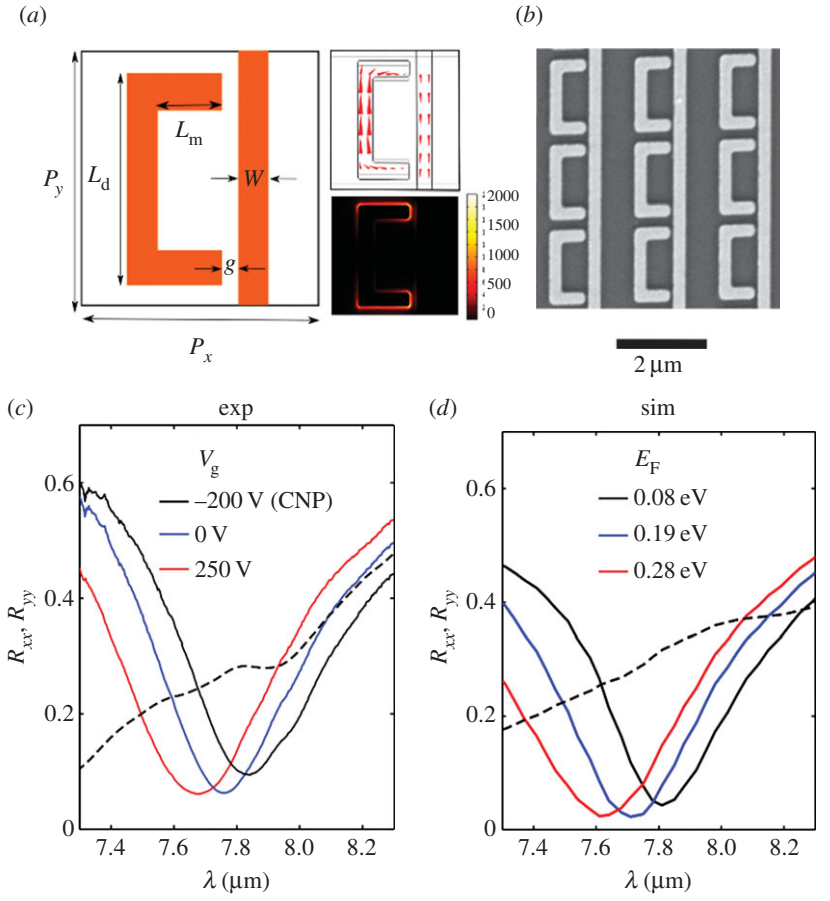

Figure 2. (*a*) Schematic and geometry definitions of a GIAM that exhibits resonant behaviour for *y*-polarized light but not for *x*-polarized light. Numerical simulations of the current distribution 5 nm above the graphene plane (top right inset) and of the near-field enhancement $\eta = |E_t^2/E_{inc}^2|$ at $z = 0$ (bottom right inset) illustrate the resonant excitation of the C-shaped plasmonic antenna. (*b*) Scanning electron microscope image of the fabricated metasurface. (*c*) Experimentally measured reflectivity for *x*-polarized light (dashed line) and *y*-polarized light (solid lines). Different colours correspond to different gate voltages V_g defined in the legend. (*d*) Numerical simulation results corresponding to (*c*). The Fermi energies E_F correspond to the gate voltages in (*c*). Panels (*a*,*b*) are from [29]. The nominal dimensions of the structure defined in (*a*) are $P_x = P_y = 2.1\,\mu m$, $W = 250$ nm, $g = 120$ nm, $L_d = 1.8\,\mu m$, $L_m = 600$ nm.

These theoretical results agree with the measured reflectivities from the metasurface for the *y*-polarized light, which is shown in figure 2*c* for the three different gate voltages V_g that approximately match the Fermi energies in figure 2*d*. The colour coding of V_g in figure 2*c* and their respective E_F in figure 2*d* is the same. The connection between $E_F(n)$ and V_g is made using the expression $n = C\Delta V/e$, where C is the capacitance per unit area of the SiO_2 spacer, and $\Delta V = V_g - V_{CNP}$, with V_{CNP} the charge neutrality point (CNP), which is experimentally found by locating the resistance maximum between the source and the drain (figure 1) as a function of the applied back-gate voltage. For our sample, it was thus experimentally determined that $V_{CNP} = -200$ V. The experimentally observed blue-shifting of the reflectivity dip from $\lambda \approx 7.8\,\mu m$ (black solid line in figure 2*c*) at the CNP point to $\lambda \approx 7.6\,\mu m$ (red solid line) at $V_g = 250$ V is around 2.6%. The physical reason for the blue-shift is the injection of holes into graphene [41]. Note that the amount of the blue-shift is in good agreement with theoretical predictions presented in figure 2*d*.

The measured and simulated R_{xx} spectra are also presented in figure 2*c*,*d*. These spectra are essentially featureless, thus confirming our earlier conjecture that the metasurface is non-resonant for *x*-polarized light for the wavelengths of our interest. The small feature that is experimentally observed at $\lambda \approx 8\,\mu m$ in figure 2*c* is due to the epsilon-near-zero (ENZ) effect that originates from the longitudinal phonon polariton of SiO_2 [45,46]. This effect is due to finite components of the incident electric field that are normal to the substrate (i.e. E_z), which are present in our experiment due to the large numerical aperture of our focusing objective (NA = 0.5). However, our simulation is performed for normal incidence. Therefore, the ENZ feature is not present in the simulated results as shown in figure 2*d*.

In our earlier work [29], we used an interferometric set-up to experimentally measure the voltage-dependent phase shift of the *x*- and *y*-polarized incident light. Based on those measurements, we conjectured the possibility of voltage-dependent polarization state control for the incident light polarized at an angle to the resonant principal axis of the metasurface. Below, we present a direct experimental evidence of such polarization control.

2. Experimental results

In order to measure the ellipticity of the reflected light, we must measures its Stokes parameters. This is accomplished using the rotating analyser set-up [6,42] shown in figure 3*a*. The set-up consists of a quantum cascade laser source of light, a polarizer, a CaF_2 beam splitter, a graphene-integrated metasurface sample biased with a DC gate voltage, an analyser and a mercury cadmium telluride (MCT) detector. The polarization state of light after reflection from the metasurface can be described by

$$\mathbf{E} = E_x\mathbf{x} + E_y\mathbf{y} = \mathrm{Re}[E_0(\cos\theta_E\,\mathbf{x} + e^{i\phi}\sin\theta_E\,\mathbf{y})e^{-i\omega t}], \tag{2.1}$$

where E_0, θ_E and ϕ are the wavelength-dependent electric field amplitude, inverse tangent of amplitude ratio of E_y to E_x, and the phase difference between E_x and E_y, respectively. The time-averaged intensity of the analysed signal measured at the detector then can be expressed [6] as follows:

$$I(E_0,\theta_E,\theta_A,\phi) = \frac{1}{2}E_0^2\left(\cos^2\theta_A\cos^2\theta_E + \sin^2\theta_A\sin^2\theta_E + \frac{1}{2}\sin 2\theta_A\sin 2\theta_E\cos\phi\right), \tag{2.2}$$

where θ_A is the analyser angle.

In all our measurements, the polarizer angle θ_P (see figure 3*a* for a definition), which determines the ratio of the incident electric field components $E_x^{(in)}$ and $E_y^{(in)}$, is set at $\theta_P = 75°$. According to the reflectivity measurements shown in figure 2*c*, this angle results in approximately equal reflected intensities of the *x*- and *y*-polarized light at the resonance wavelength (i.e. $E_x^{(in)} \approx E_y^{(in)}$). We measured the reflection intensity as a function of the wavelength by changing the analyser angle from $\theta_A = 0°$ to $\theta_A = 90°$ in steps of 22.5° as shown in figure 3*b*. A subsequent least-squares fitting of equation (2.2) to the measured data of figure 3*b* at a given wavelength determines the fitting parameters E_0, θ_E and ϕ as a function of λ. It is then straightforward to calculate the polarization state of the detected signal from equation (2.1).

The conventional representation of the polarization state of light is in terms of its Stokes parameters defined as follows: $S_0 = I_x + I_y = E_0^2$, $S_1 = I_x - I_y = E_0^2\cos 2\theta_E$, $S_2 = I_{45°} - I_{-45°} = E_0^2\sin 2\theta_E\cos\phi$ and $|S_3| = |I_{RCP} - I_{LCP}| = |E_0^2\sin 2\theta_E\sin\phi|$. Here, $I_{x,y}$, $I_{\pm 45°}$ and $I_{RCP,LCP}$ are the intensities of light that would pass through an analyser set parallel to $x\,(y)$ axes, ±45° to the *x*-axis, and through a circular RCP/LCP analyser, respectively. Therefore, the qualitative physical meaning of the Stokes parameters is as follows: S_0 represents the total light intensity, S_1 represents the degrees of linear polarization with respect to the principal axes of the metasurface, S_2 represents the degrees of linear polarization with respect to the axes tilted at 45° with respect to the principal axes, and S_3 represents the degree of circular polarization. Of particular interest is the sign of the S_2 coefficient because it indicates the orientation of the polarization ellipse. Specifically, $S_2 > 0$ means that the polarization ellipse is elongated in the first and third

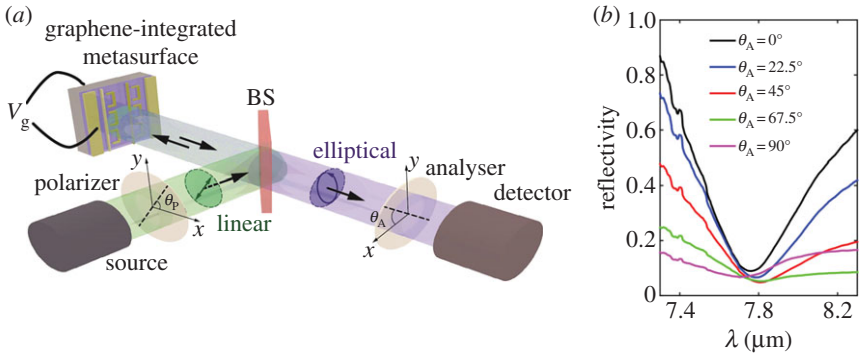

Figure 3. (*a*) The schematic for the Stokes polarimetry set-up consisting of an optical source, a beam splitter (BS), an infrared MCT detector and two linear polarizers, one after the source (polarizer) and one before the detector (analyser) of the polarization state. A graphene-integrated anisotropic metasurface controllably modulates the polarization state of the incident light when a varying gate voltage V_g is applied. (*b*) The reflectivity as a function of the wavelength for different analyser angles θ_A when the structure is illuminated with the laser light initially polarized at $\theta_P = 75°$. The gate voltage is set at $V_g = -200$ V (the CNP point) for this measurement. The source is a quantum cascade laser (QCL).

polarization quadrants, whereas $S_2 < 0$ means that the polarization ellipse is elongated in the second and fourth polarization quadrants. Note that the above calculation explicitly assumes that the reflected light is perfectly coherent, i.e. $|S_0|^2 = |S_1|^2 + |S_2|^2 + |S_3|^2$. This assumption is valid because the intensity of the reflected laser light is much higher than that of the infrared radiation thermally emitted by a heated metasurface.

A typical dependence of $I(E_0,\theta_E,\theta_A,\phi)$ on θ_A is plotted in figure 3*b* for one specific value of $V_g = -200$ V (the CNP point). Note that the ellipticity of the reflected light depends on its wavelength. For example, the reflected polarization is nearly circular around $\lambda \approx 7.75\,\mu$m because the light intensity passing through the analyser is nearly independent of θ_A. On the other hand, a significant elongation of the polarization ellipse is expected at other wavelengths, e.g. at $\lambda = 7.4\,\mu$m. We have repeated this polarimetric measurement for the same three gate voltages ($V_g = -200,\ 0,\ 250$ V) as in figure 2*c* and extracted the normalized values of the Stokes parameters, $s_1 = S_1/S_0$, $s_2 = S_2/S_0$ and $s_3 = S_3/S_0$, by fitting the experimental results to equation (2.2). The values of $\theta_E(\lambda,V_g)$ and $\phi(\lambda,V_g)$ were then extracted for those gate voltages for a wide range of laser wavelengths ($7.3\,\mu\text{m} < \lambda < 8.3\,\mu$m). The normalized Stokes parameters were then calculated from $\theta_E(\lambda,V_g)$ and $\phi(\lambda,V_g)$ and plotted in figure 4*a* with dashed (s_1), dotted (s_2) and solid (s_3) lines, respectively. The three values of the gate voltage are colour-coded using the same colour scheme as in figure 2*c*. The simulated values of the normalized Stokes parameters plotted in figure 4*b* show fairly accurate agreement with the experimental results.

The non-zero values of S_3 observed from figure 4*a* indicate that the linearly polarized incident light is converted to elliptic polarization upon reflection. This is the consequence of the different phase shifts acquired by the *x*- and *y*-polarized light. The ellipticity changes with gate voltage are observed to depend strongly on the wavelength of light. We consider two specific examples: $\lambda_1 = 7.76\,\mu$m (vertical magenta dashed line in figure 4*a*) and $\lambda_2 = 7.72\,\mu$m (vertical green dashed line in figure 4*a*). The normalized Stokes parameters at those wavelengths are obtained by reading off the values of s_i ($i = 1,2,3$) from the intersection of the $s_i(\lambda,V_g)$ curves with the corresponding vertical lines. In addition, we have plotted the gate voltage-dependent polarization ellipses for $\lambda = \lambda_1$ in figure 4*c*, and for $\lambda = \lambda_2$ in figure 4*d*. The definitions of the semi-major and semi-minor axes *a* and *b*, respectively, and the tilt angle β are shown in the inset to figure 4*b*. The tilt angle β and the ellipticity $\epsilon = a/b$ are calculated from the following equations: $\tan 2\beta = s_2/s_1$ and

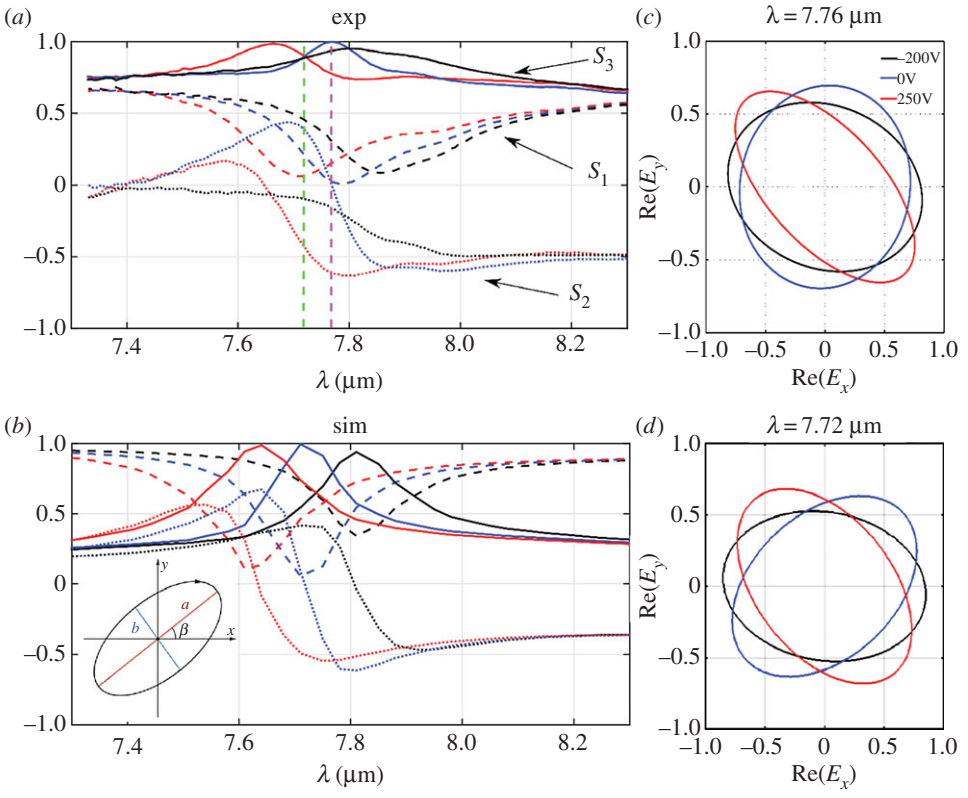

Figure 4. (*a*) Measured and (*b*) simulated normalized Stokes parameters of the reflected light as a function of the wavelength plotted for three different gate voltages. The curves are colour-coded based on the gate voltages and Fermi energies using the same convention as in figure 2*c*,*d*. (*c*,*d*) Polarization ellipses at $\lambda_1 = 7.76$ μm and $\lambda_2 = 7.72$ μm based on the measured Stokes parameters plotted in (*a*).

$\epsilon = \sqrt{\left(1+\sqrt{1-s_3^2}\right) / \left(1-\sqrt{1-s_3^2}\right)}$. Therefore, the ellipticity is controlled by a single parameter: $|s_3|$. On the other hand, the tilt angle is mainly controlled by s_2 and s_1. These observations suggest the possibility of independent control of the tilt angle and ellipticity.

For $\lambda = \lambda_1$, we observe that $s_3 = 1$ for $V_g = 0$ V, which means the reflected light is circularly polarized ($\epsilon = 1$). For the other two voltages, $V_g = -200$ V and $V_g = -250$ V, it acquires finite voltage-dependent ellipticity: $\epsilon \approx 2.1$ for $V_g = -200$ V (figure 4*c*: black ellipse) and $\epsilon \approx 4.5$ for $V_g = -250$ V (figure 4*c*: red ellipse). However, the sign of $s_2 \leq 0$ does not change with voltage. Therefore, the polarization ellipses shown in figure 4*c* remain in the second and fourth quadrants: $\beta \approx -16°$ for $V_g = -200$ V, and $\beta \approx -37°$ for $V_g = 250$ V. Note that for all three voltages $s_1 > 0$, which implies that the tilt angle of the polarization ellipse is restricted by the following inequality: $-45° < \beta < 45°$.

The $\lambda = \lambda_2$ example is particularly interesting because s_3 remains the same for all three voltages: all three solid curves in figure 4*a* intersect the green vertical line at the same value of s_3. However, the s_2 parameter changes its sign from positive for $V_g = 0$ to negative for the other two voltages. Therefore, as the gate voltage shifts from $V_g = 0$ (figure 4*d*: blue ellipse) to $V_g = 250$ V (figure 4*d*: red ellipse), the tilt angle of the fixed shape polarization ellipse shifts from $\beta \approx 31°$ to $\beta \approx -41°$ as shown in figure 4*d*. Note that $s_1 > 0$, so the tilt angle is restricted by the same condition as for the earlier case of $\lambda = \lambda_1$. The independent modulation of the tilt angle for constant ellipticity can be useful in polarization encoding and multiplexing [47].

3. Conclusion and outlook

We provide the first experimental evidence of active modulation of the polarization state of mid-infrared light using a reflective GIAM. The rotating analyser approach is used to experimentally determine the Stokes parameters of the reflected light. Polarization ellipses were experimentally obtained at several representative wavelengths for different gate voltages. Our results show that we can controllably change the polarization state of light from linear to elliptical or circular. In general, it is shown that both the tilt angle and ellipticity can be changed by injecting carriers into graphene using field-effect doping. Furthermore, it is shown that the polarization ellipse can be rotated from the first to the fourth quadrant while keeping its ellipticity constant. This modulation of tilt angle, independent of the ellipticity, can be used for polarization encoding of light and could be instrumental for improving the telecommunication bandwidth. Various applications based on field-effect GIAMs that require fast (nanosecond-scale) polarization control, such as dynamic ellipsometry, can be envisioned, and will be explored in our future work.

4. Material and methods

(a) Optical simulations

We used a commercial finite-elements solver COMSOL Multiphysics v. 4.3b to simulate the reflectivity of the sample. To model the SLG, a surface current [41] $J_{\mathrm{SLG}} = \sigma_{\mathrm{SLG}} E_{\mathrm{t}}$ was defined, where E_{t} is the tangential electric field on the SLG plane and $\sigma_{\mathrm{SLG}} = \sigma_{\mathrm{inter}} + \sigma_{\mathrm{intra}}$ is the optical conductivity of graphene that was calculated from random-phase approximation [44] as a sum of the interband and intraband contributions:

$$\left.\begin{aligned} \sigma_{\mathrm{inter}}(\omega) &= \frac{e^2}{4\hbar}\left[\frac{1}{2} + \frac{1}{\pi}\tan^{-1}\left(\frac{\hbar\omega - 2E_{\mathrm{F}}}{2k_{\mathrm{B}}T}\right) - \frac{\mathrm{i}}{2\pi}\ln\frac{(\hbar\omega + 2E_{\mathrm{F}})^2}{(\hbar\omega - 2E_{\mathrm{F}})^2 + (2k_{\mathrm{B}}T)^2}\right] \\ \text{and} \qquad \sigma_{\mathrm{intra}}(\omega) &= \frac{e^2}{4\hbar}\frac{8\mathrm{i}k_{\mathrm{B}}T}{\pi\hbar(\omega + \mathrm{i}\tau^{-1})}\ln 2\cosh\left(\frac{E_{\mathrm{F}}}{2k_{\mathrm{B}}T}\right). \end{aligned}\right\} \tag{4.1}$$

Here, k_{B} is the Boltzmann constant, $T = 300\,\mathrm{K}$ (room temperature), and the carrier scattering time of $\tau = 13\,\mathrm{fs}$ was assumed [29].

(b) Sample fabrication

SLG was grown on a polycrystalline Cu foil using a chemical vapour deposition (CVD) technique [48], then transferred [49] onto a commercially purchased Si/SiO_2 substrate (University Wafer) with 1 µm oxide layer grown on lightly doped silicon. Electron-beam patterning followed by an oxygen plasma-cleaning step isolated the high-quality graphene regions. The anisotropic metasurface with a unit cell shown in figure 2*a* was fabricated by e-beam lithography on top of SLG in an area of $100 \times 100\,\mu\mathrm{m}$, followed by lift-off. The thickness of the metasurface was 30 nm (5 nm of Cr and 25 nm of Au). Source and drain contacts 100 nm thick (15 nm Cr + 85 nm Au) were deposited on top of graphene on the two sides of the metasurface samples. Finally, a metallic contact (15 nm Ni + 85 nm Au) was deposited on the back of the silicon sample for gating. Wirebonding of the contacts to a chip carrier concluded the fabrication.

(c) Reflection measurement

The set-up shown in figure 3*a* was used to measure the optical reflectivity of the sample. The source was a quantum cascade laser (Daylight Solution, MIRcat-1400) operated in the pulsed mode with the pulse repetitions rate of 250 kHz and the pulse duration of 100 ns. A ZnSe objective lens with high numerical aperture (NA = 0.5) was used to focus the laser light onto the metasurface. A liquid-nitrogen-cooled MCT detector measured the intensity of the signal. The

measured signal was used for the measurements of signal intensity. A lock-in amplifier (Stanford Research Systems SR844) was used to amplify the measured signal with a 3 ms integration time.

Authors' contributions. S.D.-G. and G.S. conceived the experiments. N.D. performed the simulations and fabricated the sample. N.D. and S.D.-G. performed the optical measurements. S.D.-G. analysed the data. I.K. grew and transferred the CVD graphene. N.D., S.D.-G., M.A.B. and G.S. contributed to manuscript preparation. S.D.-G. and N.D. contributed equally to this project.

Competing interests. The authors declare no competing interests

Funding. This work was supported by the Office of Naval Research (ONR) Award N00014-13-1-0837 and by the National Science Foundation (NSF) Award DMR 1611379. M.A.B. acknowledges support from the Welch Foundation grant no. F-1705. We also acknowledge the assistance of Babak Fallahazad with electric characterization of the graphene sample.

References

1. Born M, Wolf E. 1999 *Principles of optics*. Cambridge, UK: Cambridge University Press.
2. Kildishev AV, Boltasseva A, Shalaev VM. 2013 Planar photonics with metasurfaces. *Science* **339**, 1232009. (doi:10.1126/science.1232009)
3. Meinzer N, Barnes WL, Hooper IR. 2014 Plasmonic meta-atoms and metasurfaces. *Nat. Photon.* **8**, 889–898. (doi:10.1038/nphoton.2014.247)
4. Yu N, Capasso F. 2014 Flat optics with designer metasurfaces. *Nat. Mater.* **13**, 139–150. (doi:10.1038/nmat3839)
5. Minovich AE, Miroshnichenko AE, Bykov AY, Murzina TV, Neshev DN, Kivshar YS. 2015 Functional and nonlinear optical metasurfaces. *Laser Photon. Rev.* **9**, 195–213. (doi:10.1002/lpor.201400402)
6. Wu C, Arju N, Kelp G, Fan JA, Dominguez J, Gonzales E, Tutuc E, Brener I, Shvets G. 2014 Spectrally selective chiral silicon metasurfaces based on infrared Fano resonances. *Nat. Commun.* **5**, 3892. (doi:10.1038/ncomms4892)
7. Arju N, Ma T, Khanikaev A, Purtseladze D, Shvets G. 2015 Optical realization of double-continuum Fano interference and coherent control in plasmonic metasurfaces. *Phys. Rev. Lett.* **114**, 237403. (doi:10.1103/PhysRevLett.114.237403)
8. Losurdo M *et al.* 2009 Spectroscopic ellipsometry and polarimetry for materials and systems at the nanometer scale: state-of-the-art, potential, and perspectives. *J. Nanoparticle Res.* **11**, 1521–1554. (doi:10.1007/s11051-009-9662-6)
9. Adato R, Yanik AA, Ansden JJ, Kaplan DL, Omenetto FG, Hong MK, Erramilli S, Altug H. 2009 Ultra-sensitive vibrational spectroscopy of protein monolayers with plasmonic nanoantenna arrays. *Proc. Natl Acad. Sci. USA* **106**, 19 227–19 232. (doi:10.1073/pnas.0907459106)
10. Morant M, Pérez J, Llorente R. 2014 Polarization division multiplexing of OFDM radio-over-fiber signals in passive optical networks. *Adv. Opt. Technol.* **2014**, 1–9. (doi:10.1155/2014/269524)
11. Zamani M, Shafiei F, Fazeli SM, Downer MC, Jafari GR. 2015 Analytic height correlation function of rough surfaces derived from light scattering. *Phys. Rev. E* **94**, 042809. (doi:10.1103/PhysRevE.94.042809).
12. Miller S. 2012 *Optical fiber telecommunications*. Amsterdam, The Netherlands: Elsevier.
13. Hao J, Yuan Y, Ran L, Jiang T, Kong JA, Chan CT, Zhou L. 2007 Manipulating electromagnetic wave polarizations by anisotropic metamaterials. *Phys. Rev. Lett.* **99**, 063908. (doi:10.1103/PhysRevLett.99.063908)
14. Pors A, Nielsen MG, Valle GD, Willatzen M, Albrektsen O, Bozhevolnyi SI. 2011 Plasmonic metamaterial wave retarders in reflection by orthogonally oriented detuned electrical dipoles. *Opt. Lett.* **36**, 1626. (doi:10.1364/OL.36.001626)
15. Wang F, Chakrabarty A, Minkowski F, Sun K, Wei Q-H. 2012 Polarization conversion with elliptical patch nanoantennas. *Appl. Phys. Lett.* **101**, 023101. (doi:10.1063/1.4731792)
16. Khanikaev AB, Mousavi SH, Wu C, Dabidian N, Alici KB, Shvets G. 2012 Electromagnetically induced polarization conversion. *Opt. Commun.* **285**, 3423–3427. (doi:10.1016/j.optcom.2012.03.023)
17. Abasahl B, Dutta-Gupta S, Santschi C, Martin OJF. 2013 Coupling strength can control the polarization twist of a plasmonic antenna. *Nano Lett.* **13**, 4575–4579. (doi:10.1021/nl4029363)

18. Li Y, Zhang J, Qu S, Wang J, Zheng L, Pang Y, Xu Z, Zhang A. 2015 Achieving wide-band linear-to-circular polarization conversion using ultra-thin bi-layered metasurfaces. *J. Appl. Phys.* **117**, 044501. (doi:10.1063/1.4906220)
19. Hao J, Ren Q, An Z, Huang X, Chen Z, Qiu M, Zhou L. 2009 Optical metamaterial for polarization control. *Phys. Rev. A* **80**, 023807. (doi:10.1103/PhysRevA.80.023807)
20. Dai Y, Ren W, Cai H, Ding H, Pan N, Wang X. 2014 Realizing full visible spectrum metamaterial half-wave plates with patterned metal nanoarray/insulator/metal film structure. *Opt. Express* **22**, 7465–7472. (doi:10.1364/OE.22.007465)
21. Chen H, Wang J, Ma H, Qu S, Xu Z, Zhang A, Yan M, Li Y. 2014 Ultra-wideband polarization conversion metasurfaces based on multiple plasmon resonances. *J. Appl. Phys.* **115**, 154504. (doi:10.1063/1.4869917)
22. Fedotov VA, Mladyonov PL, Prosvirnin SL, Rogacheva AV, Chen Y, Zheludev NI. 2006 Asymmetric propagation of electromagnetic waves through a planar chiral structure. *Phys. Rev. Lett.* **97**, 167401. (doi:10.1103/PhysRevLett.97.167401)
23. Khanikaev AB *et al.* 2016 Experimental demonstration of the microscopic origin of circular dichroism in two-dimensional metamaterials. *Nat. Commun.* **7**, 12045. (doi:10.1038/ncomms12045)
24. Yao Y, Kats MA, Genevet P, Yu N, Song Y, Kong J, Capasso F. 2013 Broad electrical tuning of graphene-loaded plasmonic antennas. *Nano Lett.* **13**, 1257–1264. (doi:10.1021/nl3047943)
25. Yao Y, Kats MA, Shankar R, Song Y, Kong J, Loncar M, Capasso F. 2014 Wide wavelength tuning of optical antennas on graphene with nanosecond response time. *Nano Lett.* **14**, 214–219. (doi:10.1021/nl403751p)
26. Si G, Zhao Y, Leong E, Liu Y. 2014 Liquid-crystal-enabled active plasmonics: a review. *Materials* **7**, 1296–1317. (doi:10.3390/ma7021296)
27. Emani NK, Chung TF, Kildishev AV, Shalaev VM, Chen YP, Boltasseva A. 2014 Electrical modulation of Fano resonance in plasmonic nanostructures using graphene. *Nano Lett.* **14**, 78–82. (doi:10.1021/nl403253c)
28. Dabidian N, Kholmanov I, Khanikaev AB, Tartar K, Tredafilov S, Mousavi SH, Magnuson C, Ruoff RS, Shvets G. 2015 Electrical switching of infrared light using graphene integration with plasmonic Fano resonant metasurfaces. *ACS Photonics* **2**, 216–227. (doi:10.1021/ph5003279)
29. Dabidian N *et al.* 2016 Experimental demonstration of phase modulation and motion sensing using graphene-integrated metasurfaces. *Nano Lett.* **16**, 3607–3615. (doi:10.1021/acs.nanolett.6b00732)
30. Zheludev NI, Plum E. 2016 Reconfigurable nanomechanical photonic metamaterials. *Nat. Nanotechnol.* **11**, 16–22. (doi:10.1038/nnano.2015.302)
31. Phare CT, Lee Y-HD, Cardenas J, Lipson M. 2015 Graphene electro-optic modulator with 30 GHz bandwidth. *Nat. Photon.* **9**, 511–514. (doi:10.1038/nphoton.2015.122)
32. Midrio M, Boscolo S, Moresco M, Romagnoli M, De Angelis C, Locatelli A, Capobianco A-D. 2012 Graphene-assisted critically-coupled optical ring modulator. *Opt. Express* **20**, 23 144–23 155. (doi:10.1364/OE.20.023144)
33. Huang F, Baumberg JJ. 2010 Actively tuned plasmons on elastomerically driven Au nanoparticle dimers. *Nano Lett.* **10**, 1787–1792. (doi:10.1021/nl1004114)
34. Kats MA, Blanchard R, Genevet P, Yang Z, Qazilbash MM, Basov DN, Ramanathan S, Capasso F. 2013 Thermal tuning of mid-infrared plasmonic antenna arrays using a phase change material. *Opt. Lett.* **38**, 368–370. (doi:10.1364/OL.38.000368)
35. Kim JT. 2014 CMOS-compatible hybrid plasmonic modulator based on vanadium dioxide insulator–metal phase transition. *Opt. Lett.* **39**, 3997. (doi:10.1364/OL.39.003997)
36. Chen H-T, Padilla WJ, Cich MJ, Azad AK, Averitt RD, Taylor AJ. 2009 A metamaterial solid-state terahertz phase modulator. *Nat. Photon.* **3**, 148–151. (doi:10.1038/nphoton.2009.3)
37. Jun YC, Brener I. 2012 Electrically tunable infrared metamaterials based on depletion-type semiconductor devices. *J. Opt.* **14**, 114013. (doi:10.1088/2040-8978/14/11/114013)
38. Shrekenhamer D, Chen W-C, Padilla WJ. 2013 Liquid crystal tunable metamaterial absorber. *Phys. Rev. Lett.* **110**, 177403. (doi:10.1103/PhysRevLett.110.177403)
39. Peng F, Chen H, Tripathi S, Twieg RJ, Wu ST. 2015 Fast-response IR spatial light modulators with a polymer network liquid crystal. *Proc. SPIE* **9384**, 93840N. (doi:10.1117/12.2081955)
40. Papasimakis N, Luo Z, Shen ZX, De Angelis F, Di Fabrizio E, Nikolaenko AE, Zheludev NI. 2010 Graphene in a photonic metamaterial. *Opt. Express* **18**, 8353. (doi:10.1364/OE.18.008353)

41. Mousavi SH *et al.* 2013 Inductive tuning of Fano-resonant metasurfaces using plasmonic response of graphene in the mid-infrared. *Nano Lett.* **13**, 1111–1117. (doi:10.1021/nl304476b)
42. Goldstein DH. 2003 *Polarized light*, 2nd edn. New York, NY: Marcel Dekker.
43. Zhang S, Genov DA, Wang Y, Liu M, Zhang X. 2008 Plasmon-induced transparency in metamaterials. *Phys. Rev. Lett.* **101**, 047401. (doi:10.1103/PhysRevLett.101.047401)
44. Falkovsky LA, Pershoguba SS. 2007 Optical far-infrared properties of a graphene monolayer and multilayer. *Phys. Rev. B* **76**, 153410. (doi:10.1103/PhysRevB.76.153410)
45. Chen D-ZA, Chen G. 2007 Measurement of silicon dioxide surface phonon–polariton propagation length by attenuated total reflection. *Appl. Phys. Lett.* **97**, 121906. (doi:10.1063/1.2789177)
46. Vasant S, Archmanbault A, Marquier F, Pardo F, Gennser U, Cavanna A, Pelouard JL, Greffet JJ. 2012 Epsilon-near-zero mode for active optoelectronic devices. *Phys. Rev. Lett.* **109**, 237401. (doi:10.1103/PhysRevLett.109.237401)
47. Gopinathan U, Naughton TJ, Sheridan JT. 2006 Polarization encoding and multiplexing of two-dimensional signals: application to image encryption. *Appl. Opt.* **45**, 5693–5700. (doi:10.1364/AO.45.005693)
48. Li X, Zhu Y, Cai W, Borysiak M, Han B, Chen D, Piner RD, Colombo L, Ruoff RS. 2009 Transfer of large-area graphene films for high-performance transparent conductive electrodes. *Nano Lett.* **9**, 4359–4363. (doi:10.1021/nl902623y)
49. Suk JW, Kitt A, Magnuson CW, Hao Y, Ahmed S, An J, Swan AK, Goldberg BB, Ruoff RS. 2011 Transfer of CVD-grown monolayer graphene onto arbitrary substrates. *ACS Nano* **5**, 6916–6924. (doi:10.1021/nn201207c)